

Figure 2: Shapes of air in frictional fluids. (a) frictional fingers (low rate, low packing fraction, high stiffness), (b) stick slip bubbles (low rate, intermediate solid fraction, low stiffness), (c) fluidized front “corals” (intermediate rate), (d) viscous fingers (high injection rate) and (e) fractures (high packing fraction).

Stick slip bubbles. Fig. 2 (b) shows a string of bubbles that have appeared in a stick slip fashion, one by one, at approximately 10 minutes intervals. The pump rate is the same as for the frictional fingers, but by either increasing the packing fraction or by increasing the compliance of the system (or both), the dynamics changes abruptly to this new dynamic mode. Each bubble scoops up a thick granular front, and breaking through this front requires a high gas pressure. In the stationary period, the constant driving of the pump compresses the gas and the pressure slowly builds until the jammed granular front finally yields. The interface yields at its weakest point, from which a narrow channel breaks through the jammed packing. The compressed gas expands, and a bubble inflates in the granular-liquid mixture.

VISCOUS REGIME

Fluidized front (corals). At flow rates greater than roughly 0.1 ml/min , the motion of the front is fast enough that fluid forces inside the packing overcome friction and prevent jamming of the front. The active front is continuously fluidized by the moving interface, and we are in a domain where viscous forces dominate the dynamics. Fig. 2 (c) shows a peculiar looking “coral” structure that grows at intermediate flow rates. The pattern develops in a two-stage process: first a bubble expands. Then narrow fingers start to invade the fluidized front surrounding the bubble. The less viscous gas penetrates the (more viscous) fluidized mixture driven by the pressure gradient across the front in a process of local viscous fingering. When one finger gets ahead of the rest, it accelerates, evolving into another bubble.

Viscous fingers. Cranking up the pump rate above 10 ml/min

results in another transition in the system: As Fig. 2 (d) shows, there is no longer a dark front of accumulated granular material surrounding the interface. The granular material is re-suspended by the flow, and we are now effectively dealing with a granular suspension. The Saffman-Taylor instability [9] in granular suspensions has been studied by other authors [3,4], and like Chevalier *et al.* [3], we find an early destabilization and branching of the viscous fingers due to the noise associated with the granularity of the suspension (Fig. 2 (d)).

SOLID REGIME

Fractures. What happens when we increase the packing fraction considerably? At $\varphi \sim 0.9$ the granular material fills the gap in the cell, but is not fully compacted into a close packed configuration. The material is a solid, yet deformable (porous) medium. Fig. 2 (e) shows that injection of gas into this system results in fractures. The fractures are several particle diameters wide, and the morphology is fractal of appearance. The fractures grow intermittently, in a stick slip fashion similar to the bubbles in Fig. 2 (b).

Porous media. If the packing fraction is increased further, the system ultimately reaches the close packing limit ($\varphi = 1$), and is effectively a consolidated porous medium. The displacement of fluid occurs in the pore space network defined by the rigid granular matrix. Local fluctuations in the threshold capillary pressures of pores, in addition to the viscous pressure gradient in the cell, determine the displacement dynamics [9-12]. There are two main pattern formation modes: Capillary fingering at low rates, where viscous forces are negligible and pores are invaded in sequence depending on their threshold capillary pressure, and viscous fingering at high rates, where

the displacement dynamics is governed by the pressure field in the cell. Capillary fingering progresses from pore to pore in random directions, forming compact structures in an invasion percolation process. Viscous fingers in porous media on the other hand follow the pressure gradient in the cell generated by the displacement of the fluid. They grow in thin branching fingers towards the edge of the cell in fractal structures that look similar to those obtained in diffusion limited aggregation (DLA) processes.

PHASE DIAGRAM

Summarizing the results, Fig. 3 shows a qualitative phase diagram of the morphologies as a function of compression rate (q) and the inverse of the packing fraction (φ^{-1}), i.e. from high to low packing fraction. Both axes are log-scale, and the phase borders are intended as “guides to the eye” only.

The medium changes character from porous medium to deformable solid to frictional fluid as the packing fraction decreases. Each of these regimes have characteristic morphologies associated with them, and at low rate these are capillary fingering (porous media), fractures (deformable media) and frictional bubbles and fingers (frictional fluids) respectively.

The fluid dynamics of granular mixtures changes character from frictional to viscous flows (fluidized front, viscous fingering) as the rate is increased, and the two-phase flow in porous media undergoes a transition from capillary to viscous fingering for increasing rate. The fracture mode seems reasonably rate-independent within the limited parameter range studied here.

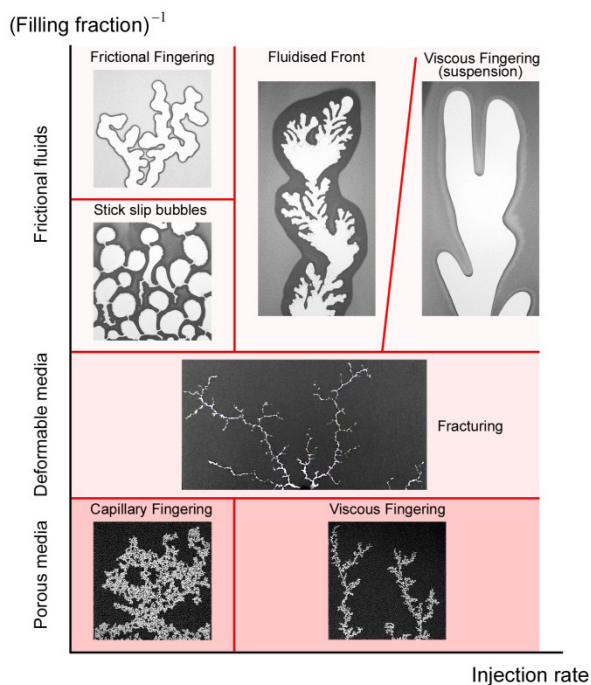


Figure 3: Phase diagram of pattern formation modes obtained by varying the packing fraction and compression rate over several orders of magnitude.

HYDROPHOBIC GRAINS

So far we have considered displacement of a granular fluid mixture by a gas. While the pattern formation is to a large degree governed by the specifics of the system, it is interesting to speculate whether the mechanisms are of a more general nature. Figure 4 shows the result of an “inverted” experiment: A layer of dry hydrophobic grains (0.1 – 0.4 mm diameter) is confined in a Hele-Shaw cell (gap ~ 0.6 mm). As water is slowly injected into the cell, the dry hydrophobic material is pushed aside by invading water fingers (seen in black in the figure). The resulting patterns and the dynamics are similar to the frictional fingering process depicted in Figure 2 (a) as it is controlled by the capillary forces at the interface, and the frictional interactions in the granular material. The specific nature of these interactions are however expected to be different (dry vs. lubricated grains, incompressibility of the invading phase etc.), and will be investigated in future work.

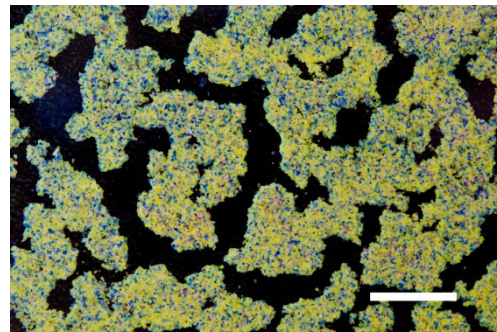


Figure 4: Fingers of water (black) penetrating dry hydrophobic granular material. Scale bar: 1 cm.


CONCLUSIONS

We find that the fluid dynamics of granular mixtures is highly complex indeed. Interactions between pressure, frictional, viscous and capillary forces conspire to produce an ever changing landscape of shapes and patterns as the experimental conditions change. Here we have presented characteristic morphologies that emerge as a result of displacement by a gas, and we have outlined the physical mechanisms at play. By mapping the displacement dynamics onto a phase diagram, we provide a means of predicting the type of dynamics occurring for a given set of conditions.

ACKNOWLEDGEMENTS

Dedicated to Henning A. Knudsen and Howard See.

- [1] X. Cheng, L. Xu, A. Patterson, H. M. Jaeger and S. R. Nagel, *Nat. Phys.* **4**, 234 (2008).
- [2] Ø. Johnsen, R. Toussaint, K. J. Måløy and E. G. Flekkøy, *Phys. Rev. E* **74**, 011301 (2006).
- [3] C. Chevalier, A. Lindner and E. Clement, *Phys. Rev. Lett.* **99**, 174501 (2007).

- [4] C. Chevalier, A. Lindner, M. Leroux, and E. J. Clement, *Non-Newton. Fluid Mech.* **158**, 63 (2009).
- [5] Ø. Johnsen, C. Chevalier, A. Lindner, R. Toussaint, E. Clément, K. J. Måløy, E. G. Flekkøy and J. Schmittbuhl. *Phys. Rev. E* **78**, 051302 (2008).
- [6] B. Sandnes, H. A. Knudsen, K. J. Måløy and E. G. Flekkøy, *Phys. Rev. Lett.* **99**, 038001 (2007).
- [7] H. A. Knudsen, B. Sandnes, E. G. Flekkøy, and K. J. Måløy, *Phys. Rev. E* **77**, 021301 (2008).
- [8] B. Sandnes, E. G. Flekkøy, H. A. Knudsen, K. J. Måløy and H. See, *Nat. Commun.* **2**, 288 (2011).
- [9] P. G. Saffman and G. Taylor, *Proc. R. Soc. London, Ser. A* **245**, 312 (1958).
- [10] K. J. Måløy, J. Feder and T. Jøssang, *Phys. Rev. Lett.* **55**, 2688 (1985).
- [11] G. Løvoll, Y. Meheust, R. Toussaint, J. Schmittbuhl and K. J. Måløy, *Phys. Rev. E* **70**, 026301 (2004).
- [12] R. Lenormand, *Physica A* **140**, 114 (1986).
- 

PIPE FLOW AS AN EXCITABLE MEDIUM

EL FLUJO DE TOBERA COMO MEDIO EXCITABLE

D. BARKLEY

Mathematics Institute, University of Warwick, Coventry CV4 7AL, UK, D.Barkley@warwick.ac.uk

The dynamics of turbulent patches (puffs) in pipe flow are related to the dynamics of action of potentials in nerve cells.

Se relaciona la dinámica de los “parches turbulentos” (“puffs”) en el flujo por tubos, con la dinámica de los potenciales de acción en células nerviosas.

PACS: Flow transition to turbulence, 47.27.Cn; action potential propagation in nervous system axons, 87.19.lb, pipe flow, 47.60.-i

INTRODUCTION

This work explores the connection between the transition to turbulence in pipe flow and the dynamics of excitable media, as exemplified by nerve cells. The primary goal is to leverage years of extensive analysis of excitable media to understand the dynamics of pipe flow. There are several active areas of research in pipe flow that can be analyzed in this context [1, 2].

Figure 1 conveys the essential message and serves to motivate this work. Two very different physical systems are shown. The first is pipe flow, Fig. 1 (a). Fluid moves through a straight pipe with a circular cross section. The pipe is considered to be sufficiently long that end effects are not important. In the quiescent, or unexcited state, flow through the pipe is laminar and individual fluid parcels move in straight lines parallel to the pipe axis. The second system is the axon of a nerve cell, Fig. 1 (b). Here in the quiescent state, or resting state, the cell membrane is polarized with the inside of the cell at a lower voltage potential than the outside. In both systems the quiescent state is stable to small, sub-threshold perturbations and hence the systems remain in the quiescent state indefinitely unless perturbed sufficiently.

Consider now the response of these systems to large, super-threshold, perturbations. For pipe flow, Fig. 1 (c), a typical perturbation might be the injection of a small jet of fluid in the upstream region of the pipe [3]. Assuming the non-dimensional flow rate is in the relevant range, a localized patch of turbulence can be created which moves down the pipe at approximately constant speed. Such a patch of turbulence is called a puff. A typical experimental measurement of a puff would be the fluid pressure near the pipe wall for example. A key point is that the strength and spatial extent of the puff are essentially constant as the puff moves down stream and these features are determined by the nonlinear dynamics of the flow and not by the initial perturbation.

Likewise, a resting nerve axon can be stimulated by the injection of current, Fig. 1 (d). The response is a pulse of depolarization, known as an action potential, which travels down the axon. The standard measurement is the membrane potential, i.e. the voltage difference between the inside and outside of the cell. As with the puff, the shape and speed of the action potential are dictated by properties of the medium and not the stimulus initiating it.

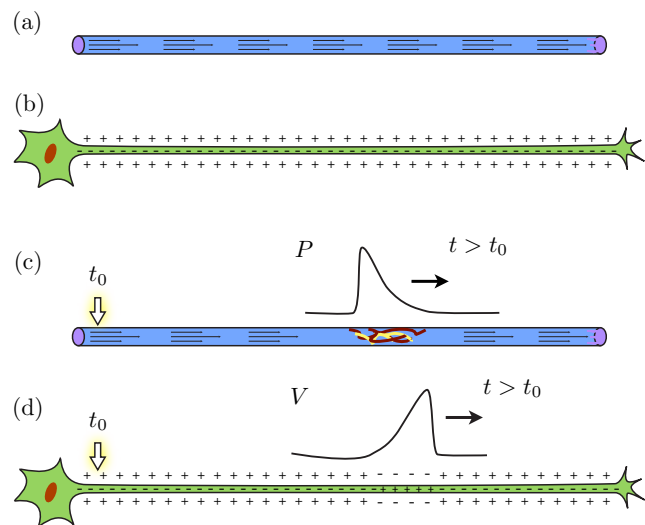


Figure 1: Cartoon illustrating the analogy between pipe flow and a nerve axon. In the absence of stimulation, both systems remain in the quiescent state: (a) flow through the pipe is laminar and (b) the axon is negatively polarized. Following an appropriate stimulation at some time t_0 , a localized patch of turbulence moves down the pipe (c) and an action potential propagates down the axon (d).

While Fig. 1 is only a cartoon, the shape of the pressure and voltage signals shown are representative of those of real systems [3, 4]. The two signals share the same features apart from the fact that they are approximately the mirror images of one another. This is not an coincidence, but rather

a manifestation of the fact that pipe flow is an excitable medium, similar in many respects to a nerve axon.

EXCITABLE MEDIA

We begin by reviewing concepts from excitable media. For the moment ignore the spatial aspects and just consider local excitable dynamics. Excitable systems are characterized as follows. (See Fig. 2.) They have a linearly stable fixed point, known as the rest state, such that small, sub-threshold perturbations of the rest state return to it without large excursion. Excitable systems additionally possess a nonlinear threshold such that super-threshold perturbations are highly amplified into what is called the excited state. The system does not remain in the excited state indefinitely, but moves into a refractory (or recovering) state and then eventually to the rest state. In the refractory phase, the system is further from the threshold than when in the rest state and hence is it more difficult to excite the system from the refractory state than from the rest state. In some cases it is impossible to excite the system directly from the refractory state. Generally the timescale associated with the nonlinear amplification into the excited state is very much faster than the time scale associated with relaxation to the rest state. The timescale associated with recovery varies considerably from system to system. (See [5, 6] for background on excitable systems.)

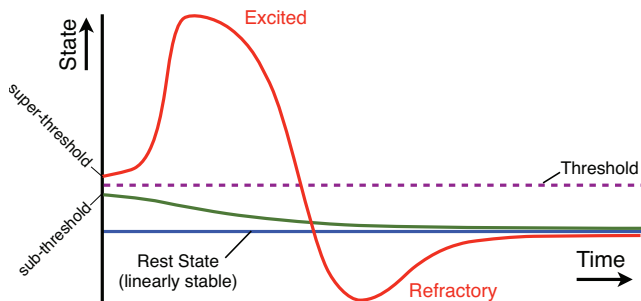


Figure 2: Schematic diagram illustrating excitability. The states of a characteristic excitable system are shown as a function of time. The rest state (blue) is a fixed point. Sub-threshold perturbations (green) of the rest state return directly to it. Super-threshold perturbations (red) are amplified into the excited state. They then go through a refractory phase before returning to the rest state.

Nerve cells are the classic example of an excitable system. The electrophysiological basis of excitability was uncovered by Hodgkin and Huxley in their groundbreaking study of squid giant axons [4]. The details are not important here, and rather than focus on the full mechanism, we consider the simplified FitzHugh-Nagumo model [7]. This model captures the essence of excitability in many physiological system and yet is amenable to straightforward analysis. In its most basic form the model is given by the following equations

$$\dot{V} = V - \frac{V^3}{3} - W + I, \quad (1)$$

$$\dot{W} = a(V + bW + c). \quad (2)$$

The variable V corresponds to membrane voltage while the variable W captures the collective effect of slow recovery of

ion channels in the cell membrane. V is called the excitation variable and W the recover variable. I represents the magnitude of a stimulus current. a , b , and c are parameters with typical values $a = 0.08$, $b = -0.8$, $c = 0.7$.

Figure 3 shows a phase portrait for the FitzHugh-Nagumo model together with illustrative trajectories. The dynamics in phase space is organized by the system nullclines: the curve on which \dot{V} and \dot{W} are zero. The V -nullcline is cubic and the middle branch is responsible for the nonlinear threshold for excitation. W provides linear negative feedback and importantly is responsible for the slow recovery. Trajectories and corresponding time series are shown for sub-threshold and super-threshold perturbations. Thus, while the model does not contain many physiological details, it does capture the essence of excitability and provides a clear geometric picture of it.

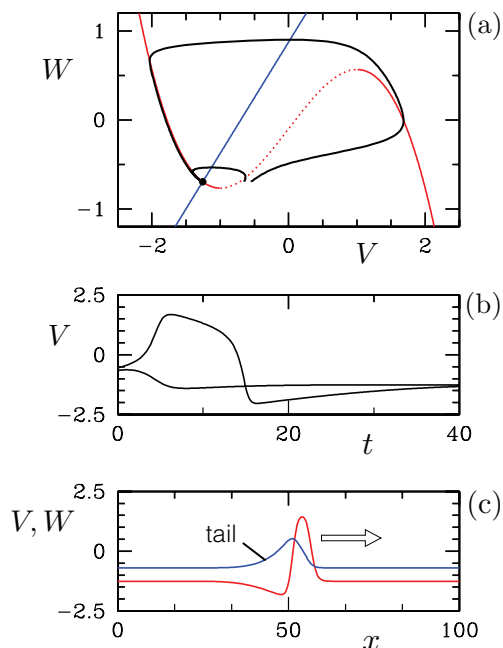


Figure 3: Dynamics of the FitzHugh-Nagumo equations. (a) Phase portrait showing the V -nullcline (red) and W -nullcline (blue) together with trajectories starting from two initial conditions. Both trajectories eventually approach the stable fixed point where the nullclines intersect. (b) Time series for the two trajectories shown in (a). (c) Action potential in the model with spatial coupling (excitable medium). Both the V (red) and W (blue) variables are plotted. A solitary pulse propagates to the right with fixed shape and constant speed. There is a refractory tail behind the pulse.

We return now to spatial aspects and excitable media. For modeling the propagation of action potentials along a nerve axon, the spatial dimension of the axon is taken into account and the FitzHugh-Nagumo model becomes

$$\partial_t V = V - \frac{V^3}{3} - W + I + \partial_{xx} V, \quad (3)$$

$$\partial_t W = a(V + bW + c), \quad (4)$$

where x represents distance along the axon. Figure 3 (c) shows a propagating action potential in the model. Once initiated, an excitation is able to sustain itself through propagation: the pulse excites adjacent medium (to the right in the figure) from

the rest state to the excited state, while at the back side of the pulse, the medium becomes un-excited, going through the refractory phase before returning to the rest state. Within the refractory tail behind the pulse it is not possible to re-excite the system.

PIPE DYNAMICS

Consider now the behavior of puffs in transitional pipe flow. Figure 4 shows a puff from direct numerical simulation of the Navier-Stokes equations [1, 8]. The flow is from left to right. A localized patch of turbulence travels down the pipe (rightward) at approximately fixed speed, maintaining approximately constant size. The two variables plotted reveal the strong similarity between puffs and the action potentials just considered: turbulent fluctuations play the role of the excitation variable while the mean flow, or mean shear, plays the role of the recovery variable.

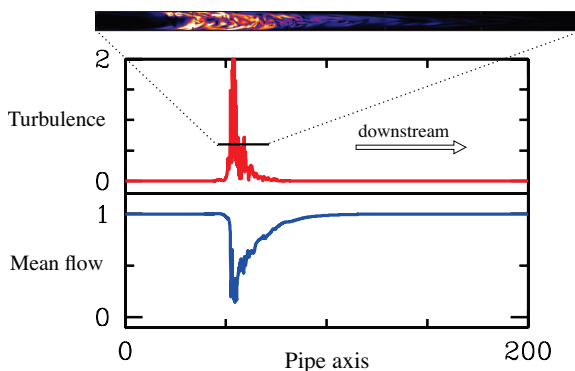


Figure 4: Puff in a direct numerical simulation of transitional pipe flow in a pipe 200 diameters long at Reynolds number 2000. The turbulent fluctuations and mean flow are sampled along the pipe axis at one instant in time. Specifically, the red curve shows the magnitude of transverse fluid velocity (scaled up by a factor of 6) while the blue curve shows the centerline velocity, relative to the mean velocity. A visualization shows the turbulent kinetic energy within the portion of the pipe containing the puff.

To better understand the connection between puffs and action potentials, consider the following model for transitional pipe flow [1]

$$(\partial_t + U\partial_x)q = q(u + r - 1 - (r + \delta)(q - 1)^2) + \partial_{xx}q,$$

$$(\partial_t + U\partial_x)u = \epsilon_1(1 - u) - \epsilon_2uq - \partial_xu,$$

where q represents the turbulent fluctuations and u represents the mean shear. The parameter r plays the role of Reynolds number and U accounts for downstream advection by the mean velocity.

The core of the model is seen in the q - u phase plane in Fig. 5 (a). The trajectories are again organized by the nullclines. The nullclines intersect in a stable, but excitable, fixed point corresponding to laminar parabolic flow. This is the rest state. The u dynamics with $\epsilon_2 > \epsilon_1$ captures in the simplest way the behavior of the mean shear. In the absence of turbulence ($q = 0$), u relaxes to $u = 1$ at rate ϵ_1 , while in response to turbulence ($q > 0$), u decreases at a faster rate dominated by ϵ_2 .

Values $\epsilon_1 = 0.04$ and $\epsilon_2 = 0.2$ give reasonable agreement with pipe flow. The q -nullcline consists of $q = 0$ (turbulence is not spontaneously generated from laminar flow) together with a parabolic curve whose nose varies with r , while maintaining a fixed intersection with $q = 0$ at $u = 1 + \delta$, ($\delta = 0.1$ is used here). The upper branch is attractive, while the lower branch is repelling and sets the nonlinear stability threshold for laminar flow. If the rest state is perturbed beyond the threshold (which decreases with r like r^{-1}), q is nonlinearly amplified and u decreases in response. The similarity to the nullclines for the FitzHugh-Nagumo system are evident.

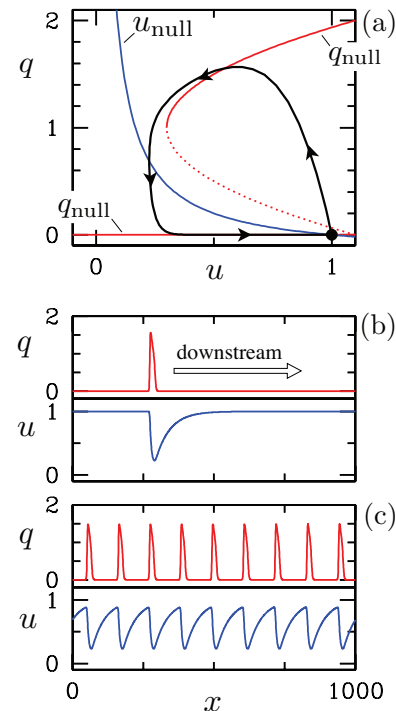


Figure 5: Puffs in the model system. (a) Phase planes shows nullclines for $r = 0.7$. The fixed point (1,0) corresponds to parabolic flow. (b) Solution snapshot at $r = 0.7$. This solution is plotted in the phase planes with arrows indicating increasing x . (c) Sequence of puffs at approximately the maximum density supported by the system.

Figure 5 (b) shows a puff in the model and should be compared both with the puff in Fig. 4 and with the FitzHugh-Nagumo action potential seen in Fig. 3. Two important properties of puffs can now be readily understood. The first concerns the shape of the puff in relationship to that of the action potential. While both structures are moving to the right, they do so for different reasons. As already stated, the action potential travels to the right by exciting the medium to its right. The refractory tail is to the left. By contrast, for the turbulent puff, the excitation from the rest state to the excited state occurs on the left side of the puff and the refractory tail is on the right side. (While not stated in these terms, the physics of this has well understood since at least 1973 [9].) The reason the puff moves to the right is due to the overall downstream motion of fluid within the pipe. This is captured by the parameter U in the model. In the absence of this downstream advection, puffs move to the left (at least for most Reynolds numbers). If experiments were routinely performed in a frame of reference in which the mean flow were zero, the shape of the puff and the

direction of propagation would be related exactly as they are for action potentials in physiological media.

The other feature that is evident from this analysis concerns the separation of adjacent puffs. It has been shown in pipe flow that the degree of recovery downstream of a puff dictates how susceptible the flow is to re-excitation into turbulence [10]. This effect is due to the refractory tails on the downstream side of puffs –the slow recovery of u in the model. If one attempts to excite a second puff closely behind a first puff, either the second puff will fail to excite, or if it does, it will either combine with the first puff or move away from it until a characteristic separation is established. Figure 5 (c) shows a number of puffs in the model. The density is at, or nearly at, the maximum supported by the medium.

CONCLUSIONS

In this short paper I have presented ideas connecting the dynamics of transitional pipe flow to the behavior of action potentials in excitable media. I have argued that these systems are closely related and that this relationship is helpful in understanding the dynamics of pipe flow. The analysis can be extended to include more realistic behavior for turbulence,

since after all, turbulence is not a single scalar quantity. Extending to other shear flows is difficult, but work as begun along these lines and appears promising [2].

-
- [1] D. Barkley, *Phys. Rev. E* **84**, 016309 (2011).
 - [2] D. Barkley, *J. Phys: Conf. Seri.* **318**, 032001 (2011).
 - [3] K. Avila, D. Moxey, A. de Lozar, M. Avila, D. Barkley and B. Hof, *Science* **333**, 192 (2011).
 - [4] A. Hodgkin and A. Huxley, *J. Physiol-London* **117**, 500 (1952).
 - [5] J. Tyson and J. Keener, *Physica D* **32**, 327 (1988).
 - [6] J. Keener and J. Sneyd, *Mathematical Physiology*, 2nd Ed. (Springer, New York, 2008).
 - [7] E. M. Izhikevich and R. FitzHugh, *Scholarpedia* **1**, 1349 (2006).
 - [8] D. Moxey and D. Barkley, *Proc. Nat. Acad. Sci.* **107**, 8091 (2010).
 - [9] I. Wygnanski and H. Champagne, *J. Fluid. Mech.* **59**, 281 (1973).
 - [10] B. Hof, A. de Lozar, M. Avila, X. Tu and T. M. Schneider, *Science* **327**, 1491 (2010).